Thin casting of silicon

Problem presented by

Aasgeir Valderhaug
Svenn Anton Halvorsen

Elkem and Teknova

Executive Summary

The Study Group problem posed by Elkem and Teknova involved a novel process for casting silicon in thin layers. At the Study Group, the participants modelled heat transfer and solidification in the silicon; and the spreading of molten silicon as it is fed into the casting apparatus. Some modificatons and alternatives to the proposed casting system were also discussed. This report contains all of the Study Group participants' findings.

Version 1.0
May 22, 2013
iii+19 pages

Report author

C. J. Cawthorn (Industrial Mathematics KTN)

Contributors

Linford Briant (University of Bristol)
John Brimlow (Rensselaer Polytechnic Institute)
Stephen Cook (University of Bath)
Megan Davies Wykes (University of Cambridge)
Ian Hewitt (University of Oxford)
Nicholas Letchford (University of Oxford)
John Ockendon (University of Oxford)
Angela Peace (Arizona State University)
Colin Please (University of Oxford)
Angel H Ramos (Universidad Completeuse de Madrid)
Marta Zagorowska (Polish Academy of Sciences)

ESGI91 was jointly organised by
University of Bristol
and
The Knowledge Transfer Network for Industrial Mathematics

Contents

1 Introduction **1**
1.1 Background 1
1.2 Problem description 1
1.3 Summary of Study Group discussions 2

2 Solidification and heat transport in the silicon layer **3**
2.1 Model construction 3
2.2 Analytical solutions 6
2.3 Numerical solution 9

3 Heat transport and water cooling **11**

4 Viscous spreading from the inlet **12**

5 Other casting approaches **15**

6 Conclusions **15**
6.1 Summary of results 15
6.2 Suggestions for future work 16

A Appendices **18**
A.1 Physical quantities and notation 18

Bibliography **19**

1 Introduction

1.1 Background

(1.1) Traditionally, silicon has been cast in large iron moulds. Although this method is simple and cheap, it is difficult to control the quality of the product. Surface oxidation, smoke, and poor control over heat transfer can cause inconsistent purity and crystal size between batches. Furthermore, production of microsilica and the need to employ moving vehicles in the process pose significant safety hazards.

Figure 1: Casting of silicon in iron moulds.

(1.2) As part of a large research project in metallurgical scale-up funded by Regional Research Fund Agder, Elkem and Teknova are experimenting with a novel method of casting silicon in thin sheets by a more continuous process. It is hoped that this process will maintain the casting speed of the traditional method (approximately 5000 kg in 10-15 minutes) while allowing much greater control of the silicon microstructure, reduced microsilica generation, and a safer casting environment. A prototype of the new system is currently being tested at Elkem's facility at Kristiansand.

1.2 Problem description

(1.3) A version of the proposed casting system is shown in Figure 2. Molten silicon is released from a reservoir onto a steel belt, which moves away from the reservoir at a controllable speed. Graphite blocks placed alongside the belt guide the flow of silicon along the belt, which is cooled from below by jets of cold water. This is intended to be the principal method of cooling the silicon, although some heat will also be lost from the surface, both to

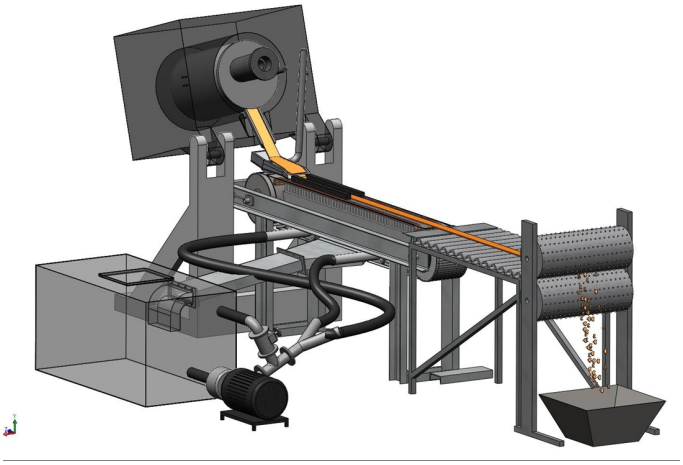

Figure 2: Illustration of the proposed casting equipment

the surrounding air and by radiation. At the end of the belt, solid silicon will be removed either by allowing it to break under its own weight, or be otherwise processed in a manner appropriate to its intended use.

(1.4) Physical quantities relevant to the problem and estimates of their values provided by Elkem are listed in Appendix A.1.

(1.5) In order to understand, improve, and scale up the prototype casting equipment, Elkem and Teknova asked the Study Group to consider the following issues.

- Given the requirement for all of the silicon to be solid by the end of the belt, how long should the belt be for a given belt speed?
- What control is possible over the temperature of the silicon at the end of the belt?
- How should the heat transfer from silicon to water be modelled? What are the effects of varying water flow and temperature?
- How do the heat transfer properties change if expansion or dust layer formation causes the contact between solid silicon and the belt to be reduced?
- How important is the method by which molten silicon is added to the belt in terms of the solification?

1.3 Summary of Study Group discussions

(1.6) At the 91st European Study Group with Industry, the problem contributors considered a range of models for sub-processes of the thin silicon casting process. Their work is described in detail in the following sections, but briefly summarised here by way of an introductory overview.

(1.7) Heavy emphasis was placed on the solidification of silicon as it moves down the interface. Both asymptotic and numerical methods were used to solve a representative Stefan problem representing the solidification, and some conclusions were drawn regarding the trends expected to be observed as the system is scaled up. The model, its solutions, and the conclusions drawn from it are presented in §2.

(1.8) Using the solidification model, it was possible to derive estimates for the heat transferred to the cooling water, as detailed in §3. If it is intended that the water does not boil, these estimates will place constraints on the operating conditions of the casting system.

(1.9) Some detailed modelling of the cross-belt spreading of molten silicon was also undertaken. This work, which is described in §4, illustrates the beginnings of an approach to investigate the effect of different inlet configurations.

(1.10) There was some discussion of some alternative casting processes used for other materials. A brief summary of these processes, and their suitability for silicon, is presented in §5.

2 Solidification and heat transport in the silicon layer

(2.1) The majority of the Study Group participants' effort was directed at the problem of solidification. The particular aim was to construct a model that could be used to draw various conclusions in response to the questions posed in §1.2.

2.1 Model construction

(2.2) The model used was for the two-dimensional steady-state system depicted by Figure 3. Molten silicon is introduced at the left-hand boundary, and is assumed to travel to the right at the speed of the belt, U_b. Cooling from above and below allows the silicon to solidify, creating two regions of solid silicon that grow along the horizontal boundaries. The solid-liquid interfaces eventually meet at some distance along the belt, beyond which the silicon is entirely solid.

(2.3) In both the solid and liquid regions, the temperature, T, of the silicon obeys the heat equation (expressed here in steady state, with constant belt speed)

$$U_b \frac{\partial T}{\partial x} = \kappa_{\mathrm{Si}} \frac{\partial^2 T}{\partial x^2} + \kappa_{\mathrm{Si}} \frac{\partial^2 T}{\partial z^2}. \tag{1}$$

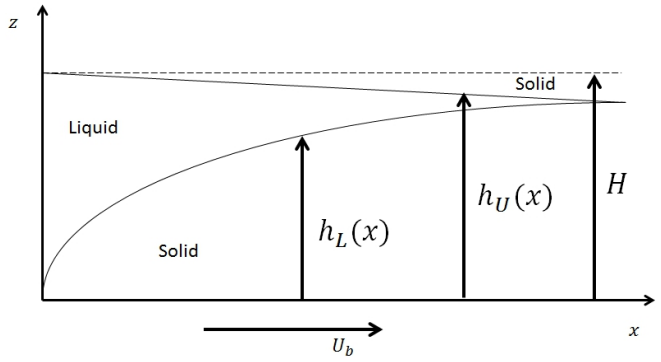

Figure 3: Diagram of solidification problem.

(2.4) On the left-hand boundary, we assume the silicon is being introduced at a constant temperature:

$$T|_{x=0} = T_0. \tag{2}$$

(2.5) On the top boundary, which is open to the air, we expect radiation to be the dominant form of heat loss. This radiative heat transfer is approximated by the boundary condition

$$-k_{\mathrm{Si}} \left.\frac{\partial T}{\partial z}\right|_{z=H} = \epsilon_s \sigma T^4. \tag{3}$$

(2.6) The silicon also loses heat to the steel belt, and through that to the cooling water. Because the belt is thin compared to the silicon layer, we chose to neglect it for the purposes of heat transfer. Instead, we consider the heat flux from the silicon to the water to be parameterised by a heat transfer coefficient, λ, thus

$$k_{\mathrm{Si}} \left.\frac{\partial T}{\partial z}\right|_{z=0} = \lambda(T - T_w). \tag{4}$$

(2.7) The upper and lower solid-liquid interfaces are located at $z = h_U(x)$ and $z = h_L(x)$ respectively. Along those interfaces, the temperature of the silicon must equal its melting temperature:

$$T|_{z=h_U} = T|_{z=h_L} = T_m, \tag{5}$$

and the Stefan condition (which accounts for the latent heat generated by a solidifying interface)

$$\rho L U_b \frac{\mathrm{d}h}{\mathrm{d}x} = \left[-k_{\mathrm{Si}} \mathbf{n} \cdot \nabla T\right]_-^+, \tag{6}$$

must be satisfied at $h = h_L$ and $h = h_U$, where $\mathbf{n}$ is the unit normal vector pointing into the solid region.

(2.8) In order to identify the key dependencies upon the physical parameters, it is helpful to nondimensionalise the equations by defining dimensionless variables (which are denoted by hats) as follows:

$$x = B\hat{x}, \quad z = H\hat{z}, \quad h_U(x) = H\hat{h}_U(\hat{x}), \quad h_L(x) = H\hat{h}_L(\hat{x}), \tag{7}$$

and

$$T(x,z) = T_w + (T_m - T_w)\hat{T}(\hat{x},\hat{z}). \tag{8}$$

This leads to the following set of equations.

$$\begin{aligned}
\mathrm{Pe}\frac{\partial \hat{T}}{\partial \hat{x}} &= \frac{\partial^2 \hat{T}}{\partial \hat{z}^2} + O\left(\frac{H^2}{L^2}\right), && (9)\\
\hat{T}|_{\hat{x}=0} &= \frac{T_0 - T_w}{T_m - T_w}, && (10)\\
\left.\frac{\partial \hat{T}}{\partial \hat{z}}\right|_{\hat{z}=1} &= -R\left(T^* + \hat{T}\right)^4, && (11)\\
\left.\frac{\partial \hat{T}}{\partial \hat{z}}\right|_{\hat{z}=0} &= \Lambda \hat{T}, && (12)\\
\hat{T}_{\hat{h}_U} &= \hat{T}_{\hat{h}_L} = 1, && (13)\\
S^{-1}\mathrm{Pe}\frac{\partial \hat{h}_U}{\partial \hat{x}} &= \left[\frac{\partial \hat{T}}{\partial \hat{z}} + O\left(\frac{H^2}{L^2}\right)\right]_{\hat{h}_U^-}^{\hat{h}_U^+}, && (14)\\
S^{-1}\mathrm{Pe}\frac{\partial \hat{h}_L}{\partial \hat{x}} &= -\left[\frac{\partial \hat{T}}{\partial \hat{z}} + O\left(\frac{H^2}{L^2}\right)\right]_{\hat{h}_L^-}^{\hat{h}_L^+}. && (15)
\end{aligned}$$

(2.9) Under the assumption that the aspect ratio H/L is small (and indeed for the test apparatus $H/L \approx 0.1$, we shall ignore the terms of order H^2/L^2.

(2.10) In equations (9-15), five dimensionless numbers appear. The most important of these is the Peclet number

$$\mathrm{Pe} = \frac{H^2 U_b}{B\kappa_{\mathrm{Si}}}, \tag{16}$$

which is the ratio of advective heat transfer (driven by the movement of the belt) to the vertical diffusive heat transfer. The Stefan number

$$S = \frac{c_{\mathrm{Si}}(T_m - T_w)}{L}, \tag{17}$$

provides the ratio of sensible heat to latent heat, and in this definition is a material property of the silicon.

(2.11) The heat transfer through the top boundary is controlled by a radiation number and a reduced temperature

$$R = \frac{\epsilon_S \sigma H (T_m - T_w)^3}{k}, \text{ and } T^* = \frac{T_w}{T_m - T_w}, \tag{18}$$

whilst the heat transfer through the steel belt is governed by a single, dimensionless heat transfer coefficient

$$\Lambda = \frac{\lambda H (T_m - T_w)}{k}. \tag{19}$$

(2.12) Although R and Λ depend on the layer depth, H, they should not be thought of as control parameters. If H were increased, then the dimensionless heat flux through each boundary would increase proportionally, but so would the heat content of the silicon layer. All that is really important is the relative strengths of radiative and conductive heating, and this is independent of H. With that in mind, it is only really Pe that are available as a control parameter for the system. This observation should be very useful when considering scale-up. Λ can also be varied by adjusting the water flow rate or temperature to change λ.

(2.13) It is worth noting that, if we assume the silicon on the belt to have an approximately constant cross-section, then the layer depth H can be estimated in terms of the volume flux Q onto the belt and the width, W, of the silicon:

$$Q \approx U_b W H \quad \Rightarrow \quad \text{Pe} \approx \frac{Q^2}{\kappa_{\text{Si}} B W^2 U_b}. \tag{20}$$

The Peclet number can therefore be tuned by controlling the volume flux, Q, and the belt speed, U_b.

(2.14) For the typical physical values provided to the Study Group by Elkem (and copied in Appendix A.1, the dimensionless parameters can be estimated as follows:

$$\text{Pe} \sim 2.4, \quad S \sim 2.5, \quad T^* \sim 0.22, \quad \text{and} \quad R \sim 0.056. \tag{21}$$

From these values, we expect that heat diffusion is about as important as heat advection and latent heat generation, and that radiative cooling is relatively weak. The dimensionless heat transfer coefficient, Λ, cannot be estimated from the available data, and should ideally be found experimentally.

2.2 Analytical solutions

(2.15) The solidification model presented in §2.1 yields analytical solutions for certain values of the dimensionless parameters. These solutions decouple the

upper and lower layers of solidifying silicon. Both of the solution approaches presented will assume that molten silicon is introduced at or near the melting point ($T_0 \approx T_m$). This allows us to assume that the temperature in the liquid layer is fixed at $T = T_m$ ($\hat{T} = 1$ in dimensionless terms).

(2.16) One can investigate the solidification of silicon from below under the assumption that radiative heating is negligible (formally setting $R = 0$), and that the heat transfer through the steel belt is very efficient (letting Λ be very large, so that $\hat{T}_{\hat{z}=0} = 0$). In this case, a similarity solution exists for the temperature distribution in the solid layer.

(2.17) Similarity solutions arise when there is no natural lengthscale to be imposed upon a system. In this case, we have both the belt length and the silicon depth to impose, so one might think a similarity solution to be inappropriate. However, since the horizontal coordinate is time-like (in the sense that information only propagates down the belt), the length of the belt ought to be irrelevant. Rather, we should find from the model the further point along the belt where liquid silicon still exists, and ensure that the belt length is longer that this. The assumption of constant temperature in the liquid layer means that the thermal problem is equivalent to one involving a semi-infinite layer of liquid silicon overlying the solidifying region, therefore the depth of silicon is also irrelevant to this part of the calculation.

(2.18) The similarity solution to the thermal problem set out in equations (9-15) takes the form

$$\hat{T}(\hat{x}, \hat{z}) = \theta(\eta), \text{ where } \eta = z\sqrt{\frac{\mathrm{Pe}}{\hat{x}}}. \tag{22}$$

The position of the solidifying interface is then given in the form

$$\hat{h}_L(\hat{x}) = \eta_0\sqrt{\frac{\hat{x}}{\mathrm{Pe}}}. \tag{23}$$

(2.19) Substituting the form of the similarity solution into the governing equations, and applying all but the Stefan condition, we eventually arrive at the solution

$$\theta(\eta) = \frac{\int_0^\eta \exp\left(-\frac{1}{4}u^2\right)\,\mathrm{d}u}{\int_0^{\eta_0} \exp\left(-\frac{1}{4}u^2\right)\,\mathrm{d}u}. \tag{24}$$

.

(2.20) Finally, the Stefan condition (15) gives us a relationship between the constant η_0 and the Stefan number

$$S^{-1}\eta_0 \int_0^{\eta_0} \exp\left(-u^2/4\right)\,\mathrm{d}u = 2\exp\left(-\eta_0^2/4\right). \tag{25}$$

For the value of S estimated in §2.1, this relationship offers a value of $\eta_0 \approx 1.054$. Armed with this value, we conclude that the silicon solidifies

from the bottom boundary according to the function

$$\hat{h}_L(\hat{x}) \approx 1.054\sqrt{\frac{\hat{x}}{\mathrm{Pe}}}. \tag{26}$$

(2.21) In the absence of cooling from the upper boundary, the silicon will have fully solidified when $\hat{h}_L = 1$. In dimensional terms, this happens when

$$x = x_{\mathrm{solid}} = 0.901 B\mathrm{Pe} = 0.901\frac{H^2 U_b}{\kappa_{\mathrm{Si}}}. \tag{27}$$

For the physical parameter values given in Appendix A.1, we estimate x_{solid} to be (rather conservatively) 6.6m. As long as the belt is longer than x_{solid}, this model predicts that only solid silicon will reach its end. If the belt length, B, is fixed, then this could be reformulated in order to specify a critical Peclet number that must not be exceeded:

$$\mathrm{Pe} \approx \frac{Q^2}{\kappa_{\mathrm{Si}} B W^2 U_b} < \mathrm{Pe}_c = 1.11. \tag{28}$$

(2.22) The notion of a critical Peclet number, expressed in the terms of (28), could be interpreted as a condition relating the belt speed and the expected volume flux of liquid silicon on to the belt. For a fixed belt speed say, the volume flux must be sufficiently small so that

$$Q^2 < \left(\kappa_{\mathrm{Si}} B W^2\, \mathrm{Pe}_c\right) U_b. \tag{29}$$

(2.23) Solidification at the upper boundary as a result of radiation can be studied in a similar way. However, the nature of the boundary condition here precludes a similarity solution. Instead, we exploit the fact that the radiation number R is small for the system under study. For small R, an expansion to linear order in R yields the solution

$$\hat{T} = 1 + R(1+T^*)^4(\hat{h_U} - \hat{z} + O(R^2) \tag{30}$$

and

$$\hat{h}_U = 1 - R\frac{(1+T^*)^4}{S^{-1}\mathrm{Pe}}\hat{x}. \tag{31}$$

(2.24) According to the small-R approximation (31), the solidifying interface near the upper surface is linear. The thickness of the layer,

$$\hat{d}_U(\hat{x}) = 1 - \hat{h}_U(\hat{x}) = R\frac{(1+T^*)^4}{S^{-1}\mathrm{Pe}}\hat{x}, \tag{32}$$

can now be added to the thickness of the lower solid region, $\hat{h}_L(\hat{x})$ to correct the estimate given in (27). x_{solid} is now the (dimensional) distance along the belt where the upper and lower solidifying interfaces meet. Using the physical parameter values supplied, we can refine our estimate of x_{solid} to 6.3m. Comparing this with our previous estimate of 6.6m, it seems clear that heat transfer through the belt is the dominant process.

(2.25) It should be noted that these solutions are approximate, and do not take account of heat transfer processes within the molten silicon. In particular, we have ignored the need to cool the silicon from its input temperature to the melting point along each of the solidifying interfaces. The Study Group participants attempted to account for this cooling in a relatively crude manner by solving the heat equation numerically in just the liquid region above the lower solid zone. The purpose of this solution was to determine the point along the free surface at which the silicon temperature dropped to the melting point, and therefore the point at which solidification could begin. This offered a very small correction to the estimate for x_{solid}.

(2.26) Furthermore, these solutions break down beyond the point at which the silicon becomes fully solid, therefore they are of limited use when trying to estimate the temperature of the solid silicon at the end of the belt. For these reasons, among others, it was necessary to solve the thermal problem numerically.

2.3 Numerical solution

(2.27) As noted in the previous section, the analytical solutions, however, attractive, are constrained by some rather large assumptions. By solving numerically, we can relax the assumption of perfect heat transfer through the belt, account for thermal diffusion within the liquid layer, and capture the interaction between the upper and lower solid regions.

(2.28) Solving a system of equations like (9-15) numerically, while simultaneously determining the unknown location of the two solid-liquid interfaces, is made difficult by the need to account for the latent heat created during solidification. Instead, it is possible to use the *enthalpy method* [1] to solve the problem without explicitly tracking the solid-liquid boundary.

(2.29) The principal idea of the enthalpy method is to solve for enthalpy, rather than temperature. Enthalpy is the sum of sensible and latent heat present in the material. If latent heat is measured relative to the solid phase, then enthalpy is defined as

$$v = \begin{cases} \rho_s c_s (T - T_m) & \text{for } T < T_m \,(\text{solid}), \\ \rho_l c_l (T - T_m) + \rho_l L & \text{for } T > T_m \,(\text{liquid}). \end{cases} \tag{33}$$

The parameters $\rho_{s/l}$ and $c_{s/l}$ denote the density and specific heat of the solid and liquid phases, respectively.

(2.30) Enthalpy is governed by the same heat equation as temperature, but it naturally includes the Stefan condition by virtue of accounting for the difference in latent heat between the liquid and solid phases. It is then a simple matter to convert the boundary conditions on temperature to conditions on

enthalpy and solve the modified set of equations. Having done so, we can recover the temperature using the relationship

$$T = \begin{cases} T_m + \frac{v}{\rho_s c_s} & \text{for } v < 0 \,(\text{solid}), \\ T_m & \text{for } 0 < v < \rho_l L \,(\text{interface}), \\ T_m + \frac{v - \rho_l L}{\rho_l c_l} & \text{for } v > \rho_l L \,(\text{liquid}). \end{cases} \tag{34}$$

The conversion between enthalpy and temperature is illustrated in Figure 4. Having determined the temperature throughout the material, the solid-liquid interface can be found by locating the $T = T_m$ contour.

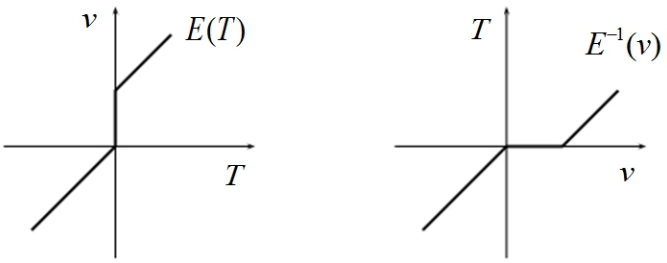

Figure 4: Illustration of the relationship between temperature and enthalpy.

(2.31) At the Study Group, participants implemented a version of the enthalpy method to find the steady solution to the problem described by equations (9-15). Using a simple, explicit finite difference scheme required the use of a very small stepsize in the horizontal direction. Furthermore, it proved difficult to maintain numerical stability in the code using the physical values relevant to silicon casting. Nevertheless, the code did allow a qualitative investigation of the system.

(2.32) A typical temperature plot obtained from the enthalpy method is shown in Figure 5. In this plot, we can clearly see the effects of conductive cooling at the bottom and radiative cooling at the top. The liquid core quickly cools from T_0 to a roughly uniform temperature a little above T_m. The solid silicon, however, exhibits a much stronger temperature gradient due to the cooling action of the horizontal boundaries.

(2.33) Note that solidification from the bottom boundary does not begin immediately, rather the material travels a little way along the belt before cooling to melting point. This is a consequence of using a finite Λ in (12) - something that was difficult to achieve in the analytical solution. As Λ is allowed to decrease, the solidification from below will be retarded further.

(2.34) After the two solid regions meet (at $x \approx 2.5$ in Figure 5), the temperature in the solid silicon begins to decrease exponentially along the belt. This

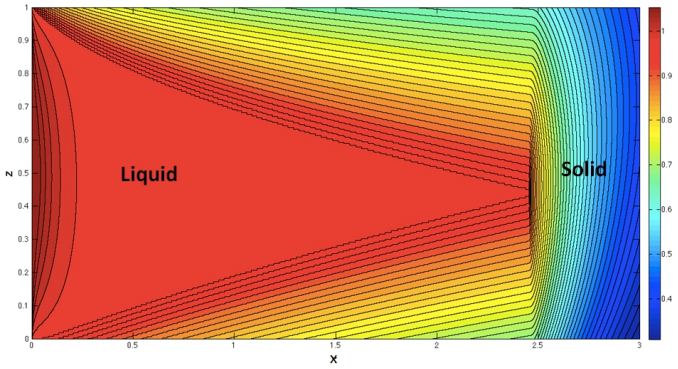

Figure 5: Qualitative temperature plot obtained from the enthalpy-based numerical code, with non-perfect heat transfer at the lower boundary ($\Lambda = 1$, $R = 4$). Black lines denote temperature contours.

may be because there is no longer any latent heat generated in the interior of the silicon, but the cooling from above and below continues unabated. If the intention is to maintain a relatively high silicon temperature at the end of the belt, then this transition from partial to full solidification should be carefully modelled, whether with more careful numerics or a more advance analytical study.

3 Heat transport and water cooling

(3.1) Having gained some insight into the thermal processes governing solidification in the silicon, we can use the model developed to explore the consequences for the heat transfer to the steel belt and cooling water. This is an important consideration for the practical operation of the new thin casting process. If the steel becomes too hot ($> 500K$, approximately), then it will suffer damage and need frequent replacement. If the cooling water is heated to near its boiling point, then steam will be produced, not only decreasing the efficiency of heating, but also requiring further containment.

(3.2) In the model constructed during the Study Group, the thermal behavior of the steel belt was neglected on the grounds that it is both thin and a good conductor of heat. A more detailed model must be constructed to include heating in the belt itself.

(3.3) The heat transfer to the water can be estimated under the assumption that all heat lost from the lower boundary of the silicon layer is used to heat the water. If the water is raised to a temperature $T_{\text{out}}(x)$, then the change in heat content of the water can be expressed as

$$\rho_w c_w Q_w (T_{\text{out}} - T_w) \approx k_{\text{Si}} \left. \frac{\partial T}{\partial z} \right|_{z=0}, \tag{35}$$

where Q_w is the volume flux of water per unit area of the belt.

(3.4) Given the heat flux $k_{\mathrm{Si}}\partial T/\partial z$ at the base of the silicon from one of the calculations in §2, equation (35) can be used to estimate the temperature change in the water. However, we note that, for the analytical solution obtained for infinite Λ, this flux diverges as $x \to 0$ because of the unrealistic assumption of perfect heat transfer.

(3.5) In order to obtain a realistic estimate of the water heating, it is necessary to use a more realistic value for the heat transfer coefficient λ. This requires that we turn to the numerical calculations described in §2.3. Although an estimate of the heat transfer coefficient was not available, it is possible to find numerical solutions for a range of values of λ. The resulting heat flux profiles are shown in Figure 6

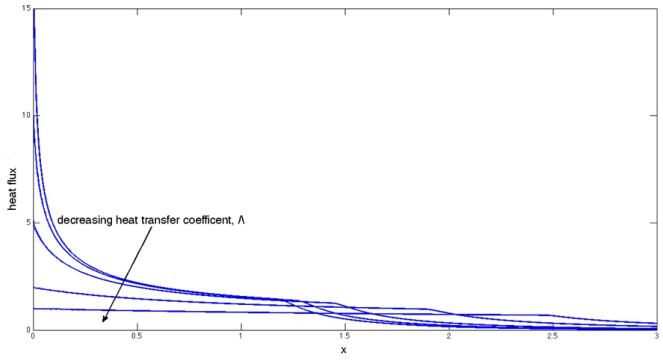

Figure 6: Plot of the heat flux through the steel belt as a function of distance along the belt for various values of Λ.

(3.6) The numerical results, which once again do not perfectly reflect the physical regime supplied, can be used to characterise the qualitative behaviour of the heat flux as Λ decreases. Smaller values of Λ seem to result in finite heat flux for small values of x, while larger (yet finite) values show some divergence near $x = 0$. In order to properly understand the heat flux here, it will be necessary to perform some detailed calculations near the start of the belt. This will most likely be achieved with some more careful numerical calculations.

4 Viscous spreading from the inlet

(4.1) In the prototype setup, Elkem have observed some variation in the cross-sectional shape of the product. In some cases, the surface is mostly flat, but slightly convex. In others, it is concave at the edges that would have been in contact with the graphite blocks. When designing an inlet to use in

a production setting, Elkem would like to understand the way in which the molten silicon can be expected to spread across the belt depending upon the shape and size of the inlet channel, as well as the vertical separation between the end of the channel and the belt.

(4.2) If we assume that the critical Peclet number condition (28) is being met, then the belt speed should be high relative to the flow of silicon down the inlet channel, making the belt speed the dominant fluid velocity scale. The reduced Reynolds number for the flow is then

$$\mathrm{Re}_\delta = \frac{H^2}{W^2}\frac{\rho_{\mathrm{Si}} W U_b}{\mu_{\mathrm{Si}}} \approx 2.67 \times 10^{-}1 \tag{36}$$

where W, the width of the belt, is used as the horizontal lengthscale. This relatively small value for the Reynolds number means that the modelling can be simplified significantly by neglecting inertia and assuming that the liquid motion is driven only by gravity and viscous drag from the belt.

(4.3) More specifically, a small reduced Reynolds number allows the use of lubrication theory to model the spreading of the liquid silicon, as described by [2]. Under lubrication theory, it is possible to separate variation on the short vertical lengthscale from variation on the long horizontal lengthscale when determining the fluid velocity. An evolution equation for the depth, H, of the silicon, can then be found by depth-integrating the conservation of mass.

(4.4) For the case of silicon spreading on a moving belt, a lubrication treatment almost identical to that of [2] tells us that the local mass flux is given by

$$\mathbf{q} = U_b \hat{\mathbf{x}} - \frac{\rho_{\mathrm{Si}} g H^3}{12\mu_{\mathrm{Si}}} \nabla H, \tag{37}$$

where $\hat{\mathbf{x}}$ is the unit vector in the direction of the belt. Conservation of mass ($\nabla \cdot \mathbf{q} = 0$) then gives us an equation for the steady depth of silicon:

$$U_b \frac{\partial H}{\partial x} = \frac{\rho_{\mathrm{Si}} g}{12\mu_{Si}} \nabla \cdot \left(H^3 \nabla H \right). \tag{38}$$

(4.5) If the lateral extent of the silicon is represented by the curves $y = \pm s(x)$, then we require that the fluid depth falls to zero there, thus

$$H(x, s(x)) = H(x, -s(x))) = 0. \tag{39}$$

Furthermore, if we assume that a constant volume flux, Q, of material is supplied to the belt, then global conservation of mass requires that

$$Q = \int_{-s(x)}^{s(x)} q_y(x, y)\, \mathrm{d}y \qquad \text{for all } x. \tag{40}$$

(4.6) If one makes the further assumption that cross-belt variations occur on a much shorter lengthscale than down-belt variations, then one can approximate (38) by

$$\frac{12U_b\mu_{\mathrm{Si}}}{\rho_{\mathrm{Si}}g}\frac{\partial H}{\partial x} = \frac{\partial}{\partial y}\left[H^3\frac{\partial H}{\partial y}\right], \tag{41}$$

and (40) by

$$Q = U_b\int_{-s(x)}^{s(x)} H(x,y)\,\mathrm{d}y. \tag{42}$$

This set of equations, along with the boundary condition (39), admits the similarity solution

$$H(x,y) = \frac{1}{x^{1/5}}\left(\frac{18U_b\mu_{\mathrm{Si}}}{5\rho_{\mathrm{Si}}g}\right)^{1/3}\left[\alpha^2 - \left(\frac{y}{x^{1/5}}\right)^2\right]^{1/3}, \tag{43}$$

where

$$\alpha = \frac{\frac{Q}{U}\left(\frac{5\rho_{\mathrm{Si}}g}{18U_b\mu_{\mathrm{Si}}}\right)^{1/3}}{\int_{-1}^{1}(1-\psi^2)^{1/3}\,\mathrm{d}\psi}. \tag{44}$$

This solution is illustrated by Figure 7.

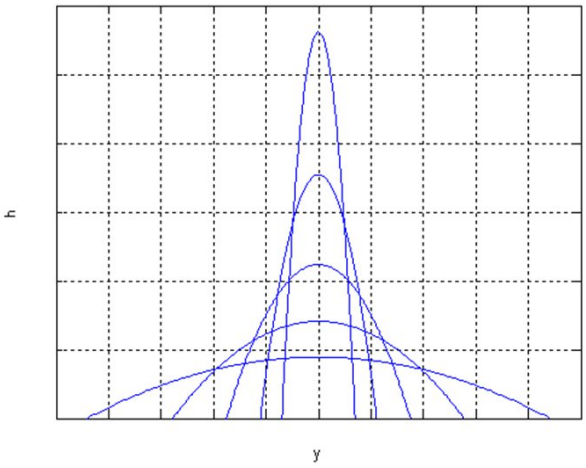

Figure 7: Similarity solution (43) for the depth of spreading silicon, $H(x,y)$, shown as a function of y for several fixed values of x.

(4.7) The similarity solution (43) will break down when the flow reaches the insulating blocks on each side of the belt, because the assumption of self-similarity will be violated. In order to properly explore the behaviour of the flow, it will be necessary to solve numerically in a manner that accounts for the side walls explicitly.

(4.8) It is important to note that no account of thermal affects has been made in this calculation. To fully model the behaviour of the molten silicon, one ought to account for the possibility that some silicon will solidify very soon after it hits the belt. Although this was not attempted by the Study Group, the reader may wish to consult more recent works (e.g [3], [4], [5] or [6]), who obtained some analytical results for a similar problem.

5 Other casting approaches

(5.1) There was some brief discussion at the Study Group about other casting methodologies used for other materials. Specifically, it was noted that the steel industry has been using and refining similar continuous casting apparatus for several decades. Although steel and silicon have very different physical properties - most notably, that steel is ductile where silicon is rather brittle - it may be that a detailed survey of the methods and literature surrounding steel casting would yield some useful information.

(5.2) Float glass manufacture may also provide some useful insights into continuous casting of silicon. The float glass method replaces the steel belt of the silicon system with a reservoir of molten metal, usually tin. Molten glass (which has a melting point about 200K smaller than silicon) is poured on to the surface of the tin and spreads to form a smooth ribbon. It is then removed from the tin and gradually cooled in a kiln until it solidifies. The gradual cooling is essential to ensure that the glass does not crack upon cooling. It is likely that this kind of process carries too high an energy cost to be viable to silicon casting, but the physical insights it may give into material stresses and strain under cooling may be relevant to the solidification of silicon.

(5.3) As an alternative to the inlet channel, the possibility of using a curtain coating method was suggested. In curtain coating, a reservoir of molten material would be held above the belt. Molten silicon would be allowed to fall from a slot in the bottom of the reservoir onto the belt in a way that minimises variation across the belt. This would improve the consistency of flow onto the belt, but perhaps at the cost of increases oxidation, as the silicon spends more time in contact with the air.

6 Conclusions

6.1 Summary of results

(6.1) At the 91st European Study Group with Industry, the participants attempted to model continuous thin silicon casting by focussing mainly on the process of solidifcation as the silicon moves along the belt. A clear mathematical model has been formulated and solved analytically in the case of

perfect heat transfer through the belt. This crude approximation suggests that all of the silicon should have solidified by the time it has reached a distance of approximately 1m from the inlet. More realistic heat transfer can be handled numerically. The Study Group recommends the use of an enthalpy-based method for the numerical calculation, because it avoids the need to explicitly track the solidifying interface.

(6.2) Some attention was paid to the amount of heat transferred through the belt into the cooling water. The Study Group has demonstrated a means of estimating the temperature change in the cooling water based on the solution to the solidification model, but some modelling, estimation or measurement of the heat transfer coefficient through the belt must be made in order to arrive at a quantitative estimate of the temperature change. Much the same can be said of the temperature change in the steel belt, although some additional modelling will be necessary in this case.

(6.3) The Study Group has demonstrated that, provided that the flow from the inlet is sufficiently slow, the molten silicon should flow according to the equations of lubrication theory. An evolution equation for the shape of the silicon flow was presented, and was solved analytically in a special case. Treatment of more realistic geometry will likely require numerical modelling.

(6.4) Finally, the Study Group recommended that the methods used in continuous casting of steel and glass could be investigated, on the grounds that they may offer useful insights for the process of thin casting of silicon.

6.2 Suggestions for future work

(6.5) There are many ways in which the work of the Study Group participants could be built upon. The solidification problem would benefit strongly from a more sophisticated numerical treatment. Given the way in which enthalpy exhibits a discontinuity along the solidifying interface, the numerical scheme used ought to be able to capture such a discontinuity accurately. Implicit timestepping, shock-capturing modifications, central-upwind schemes and many more techniques may be used to achieve this goal.

(6.6) It is important to realise that no account has been made of density variations within the silicon. It is possible that the cooler temperatures near the upper solidifying interface may give rise to onvection, which will act to homogenise the temperature in the interior and create sharper temperature gradients near the solid-liquid interfaces. Homogenisation could be enhanced by relatively buoyant pieces of solid silicon breaking off from the belt and floating toward the surface, mixing the liquid silicon as they rise. Such mixing effects are likely to retard the solidification process, meaning that our prediction of 1m is likely to be an underestimate. Furthermore, solid silicon is about 10% less dense than molten silicon. The expansion

that results from cooling will have an effect on the size of the solid layers, and also impact upon the behaviour of both temperature and phase as the silicon moves along the belt.

(6.7) Further study of heat transfer through the belt will be useful in understanding both the risk of damage to the belt and the potential for control that can be exerted by varying the flow rate of the cooling water. This problem seems amenable to theoretical study in its simplest form, but will be complicated by the presence of dust layers or loss of contact due to thermal expansion. Experimental studies of heat transfer may be profitable.

(6.8) The initial steps made towards understanding the inlet flow could be expanded upon by performing a more detailed study in particularly geometries of interest. Furthermore, the fluid spreading should be coupled to the solidification processes, perhaps building on the works cited in §4. If it proves necessary to introduce silicon at a sufficiently large fluid velocity as to make the reduced Reynolds number large, then the lubrication model should be abandoned in favour of a more complicated fluid model for moderate Reynolds numbers. Note that the concave shape observed in the second experimental run should not appear for low Reynolds number flow.

A Appendices

A.1 Physical quantities and notation

(A.1) Table 1 contains a list of all of the physical parameters used in modelling thin silicon casting. In the main text, these values appear without definition. Other variables should be defined in situ, with hats denoting dimensionless variables.

Name	**Notation**	**(Approximate) value**
Belt length	B	$\sim 3\,\mathrm{m}$
Silicon layer depth	H	$\sim 6 - 30\,\mathrm{mm}$
Steel belt thickness	D	$\sim 0.5\,\mathrm{mm}$
Belt width (between graphite blocks)	W	$\sim 0.1\,\mathrm{m}$
Belt speed	U_b	$\sim 10\,\mathrm{m\,min^{-1}}$
Input temperature of Si	T_0	$\sim 1800\,\mathrm{K}$
Melting point of Si	T_m	$\sim 1685\,\mathrm{K}$
Input temperature of cooling water	T_w	$\sim 300\,\mathrm{K}$
Density of liquid Si	ρ_{Si}	$\sim 2 \times 10^3\,\mathrm{kg\,m^{-3}}$
Density of water	ρ_{w}	$\sim 1 \times 10^3\,\mathrm{kg\,m^{-3}}$
Thermal conductivity of Si	k_{Si}	$40\,\mathrm{W\,m^{-1}\,K^{-1}}$
Specific heat of Si	c_{Si}	$970\,\mathrm{J\,kg^{-1}\,K^{-1}}$
Specific heat of water	c_w	$4187\,\mathrm{J\,kg^{-1}\,K^{-1}}$
Thermal diffusivity of Si	κ_{Si}	$\sim 2.1 \times 10^{-5}\,\mathrm{m^2\,s^{-1}}$
Latent heat of fusion of Si	L_{Si}	$\sim 2 \times 10^6\,\mathrm{J\,kg^{-1}}$
Dynamic viscosity of Si	μ_{Si}	$\sim 0.75\,\mathrm{kg}\,m^{-1}\,s^{-1}$
Surface emissivity	ϵ_S	~ 0.5
Stefan-Boltzmann constant	σ	$5.67 \times 10^{-8}\,\mathrm{W\,m^{-2}\,K^{-4}}$

Figure 1: Table of physical parameters and constants.

Bibliography

[1] Voller, V. and Cross, M. (1981) Accurate solutions of moving boundary problems using the enthalpy method,*Int. J. Heat Mass. Tran.*, **24**, 545-556.

[2] Huppert, H. E. (1982) The propagation of two-dimensional and axisymmetric viscous gravity currents over a rigid horizontal surface, *J. Fluid Mech.*, **121**, 43-58.

[3] Balmforth, N. and Craster, R. (2000) Dynamics of cooling domes of viscoplastic fluid, *J. Fluid Mech*, **422**, 225-248.

[4] Bunk, M. A. and King, J. R. (2003) Spreading melts with basal solidification, *Z. Angew. Math. Mech.*, **83**, 820-843.

[5] Smith, W. R. (2004) The propagation and basal solidification of two-dimensional and axisymmetric viscous gravity currents, *J. Engng. Math.*, **50**, 359-378.

[6] Fink, J. H. and Griffiths, R. W. (1990) Radial spreading of viscous gravity currents with solidifying crust, *J. Fluid Mech*, **221**, 485-509.